

**Mantle flow models with core-mantle  
boundary constraints support evidence  
for chemical heterogeneities in the  
lowermost mantle**

*Bernhard Steinberger*

Bayerisches Geoinstitut  
Universität Bayreuth, Germany

*Richard Holme*

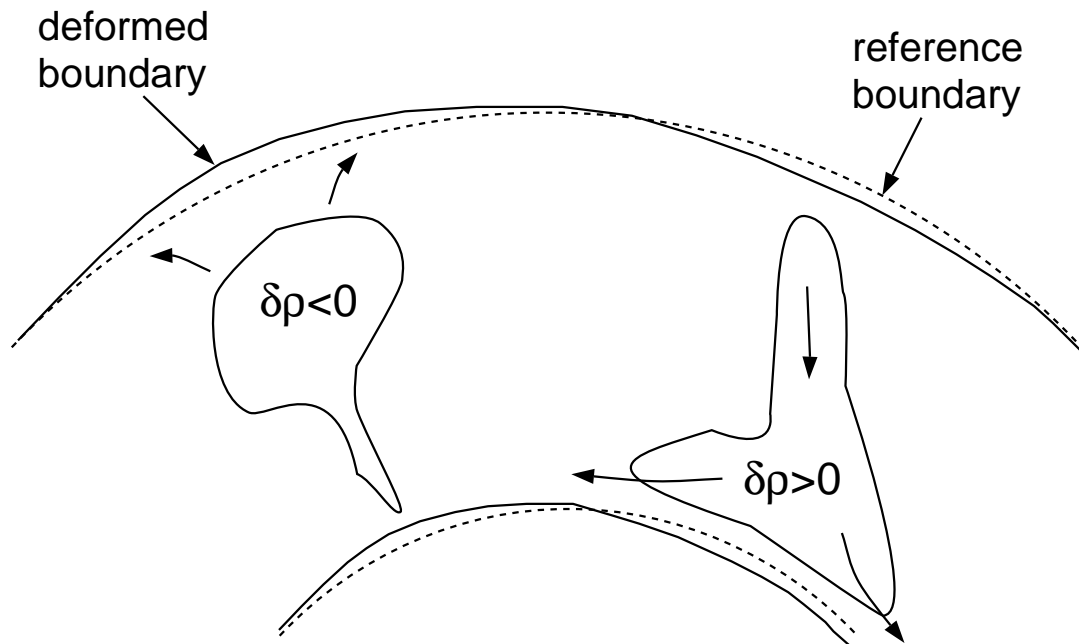
Department of Earth Sciences,  
University of Liverpool, U.K.

## Overview

- Mantle flow models based on s-wave tomography models and constrained by geoid, global heat flux, postglacial rebound tends to over-predict CMB excess ellipticity and long-wavelength r.m.s. CMB topography
- Bulk sound and shear wave anomalies decorrelate in the lowermost mantle.

In an effort to obtain a better fit to core-mantle boundary constraints, we construct a flow model that is based on both s-wave and bulk sound tomography models, and contains a distinct chemical layer at the base of the mantle

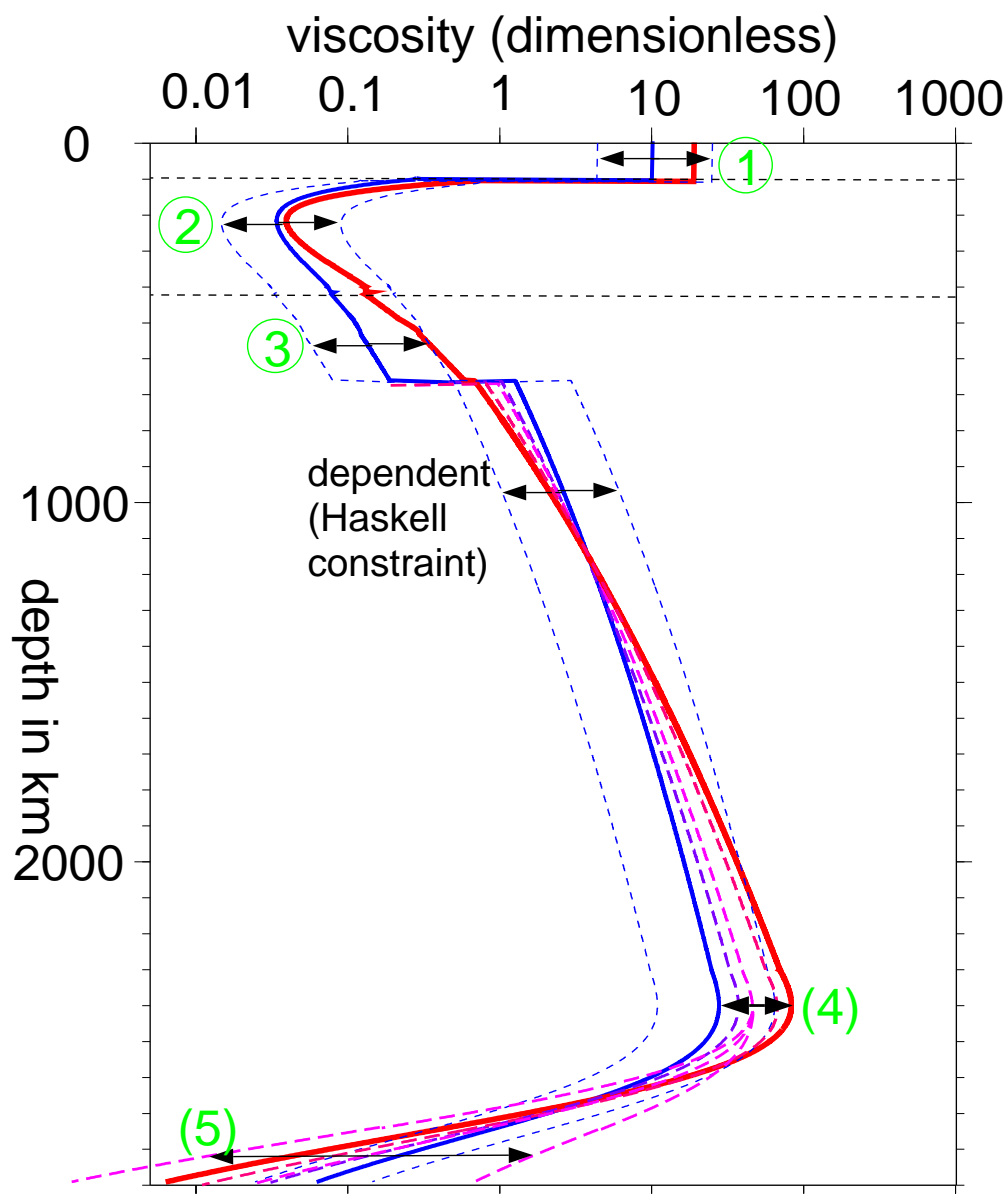
# Computation of mantle flow field, boundary deformations and geoid



- Density anomalies (inferred from tomography models) drive flow, computed with spectral method (Hager and O'Connell, 1981)
- Flow deforms boundaries
- Density anomalies and deformed boundaries contribute to geoid anomalies (Richards and Hager, 1984)

# Viscosity structure; free model parameters

- assume viscous rheology, radial viscosity variations only
- relative viscosity variations in each layer (upper mantle, transition zone, lower mantle) based on Calderwood (1999)



# Optimizing the model

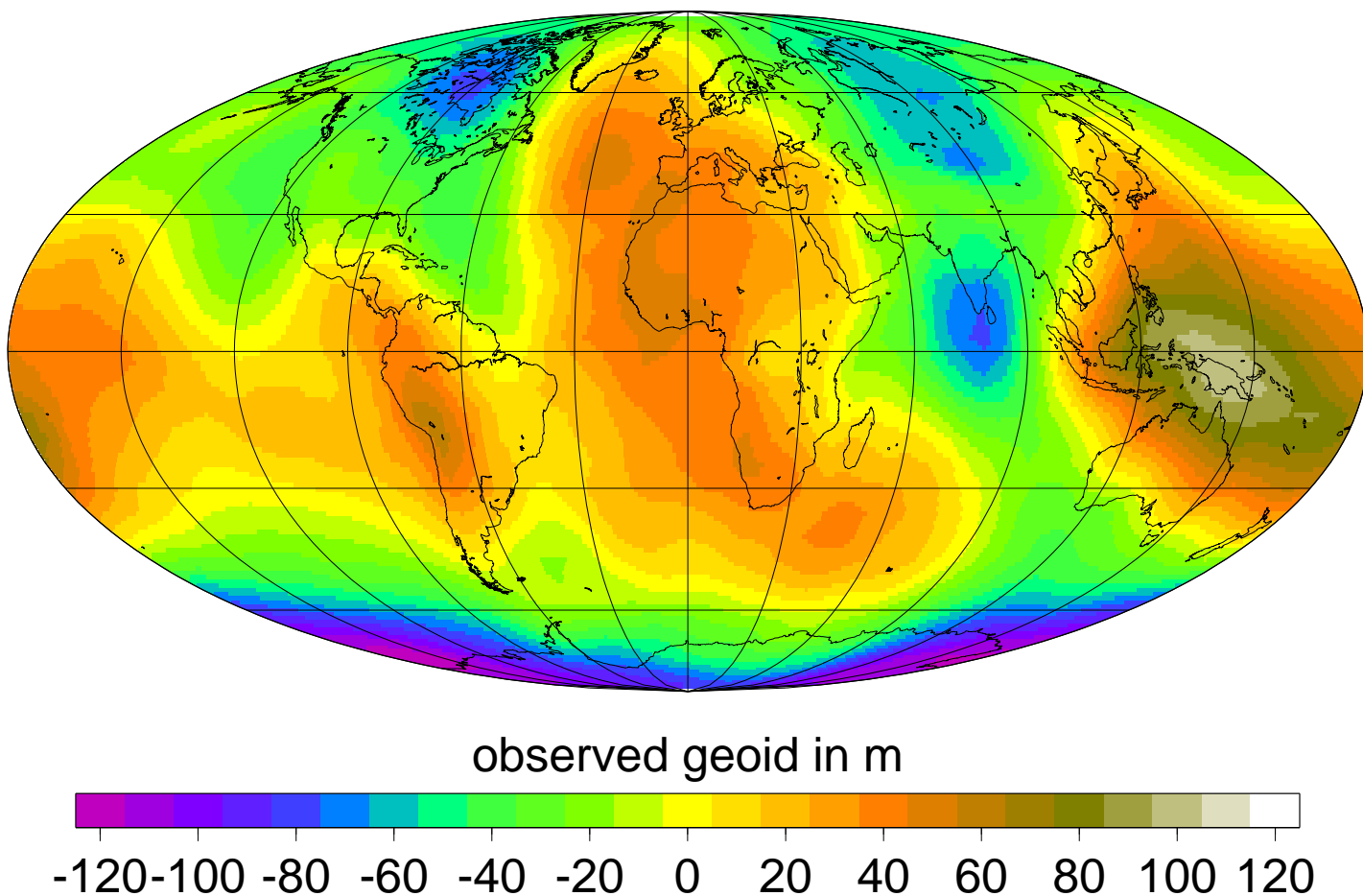
Try to minimize  $MF = MF(1) + \dots + MF(n)$ , where  $MF(i)$  describe “misfit” to various observations

## 1. Geoid

Use variance reduction

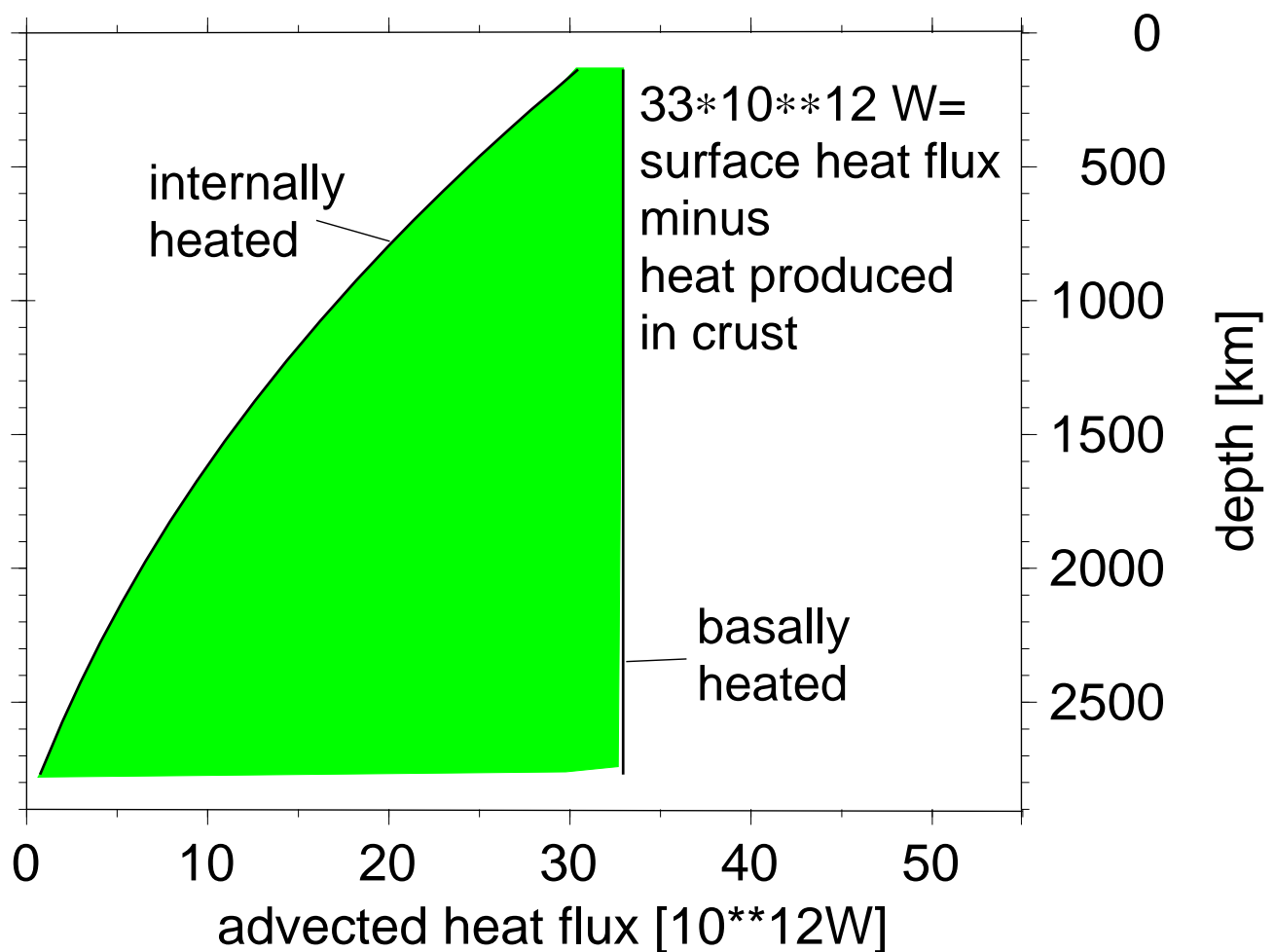
$$VR = \left( 1 - \frac{\text{Var}(\text{Predicted} - \text{Observed})}{\text{Var}(\text{Observed})} \right)$$

to describe fit;  $MF(1) = -VR$



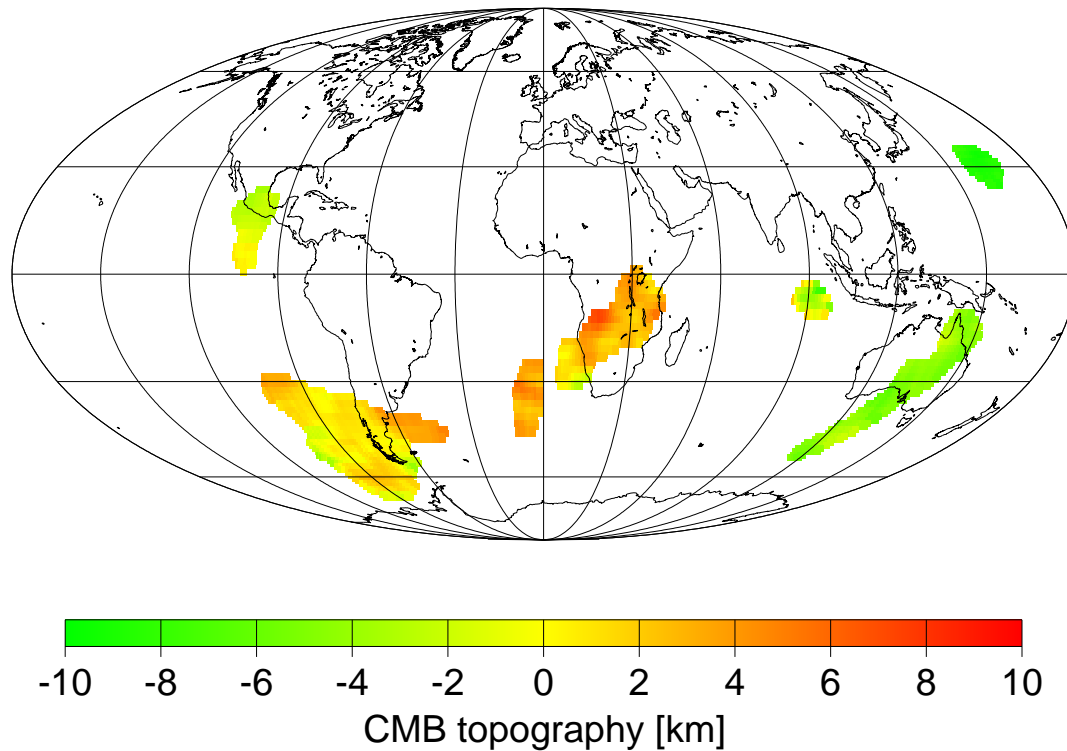
## 2. Heat flux profile

Computed based on density anomaly, flow, thermal expansivity and heat capacity.  $MF(2) > 0$ , if part of the computed curve is not in green area



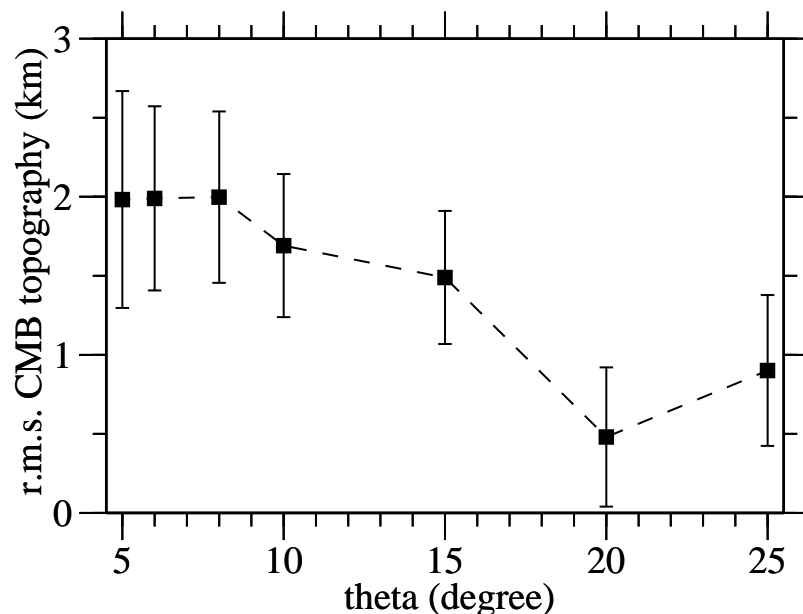
### 3. CMB constraints

#### A. Topography point constraints



from R. Garcia (pers. comm.)

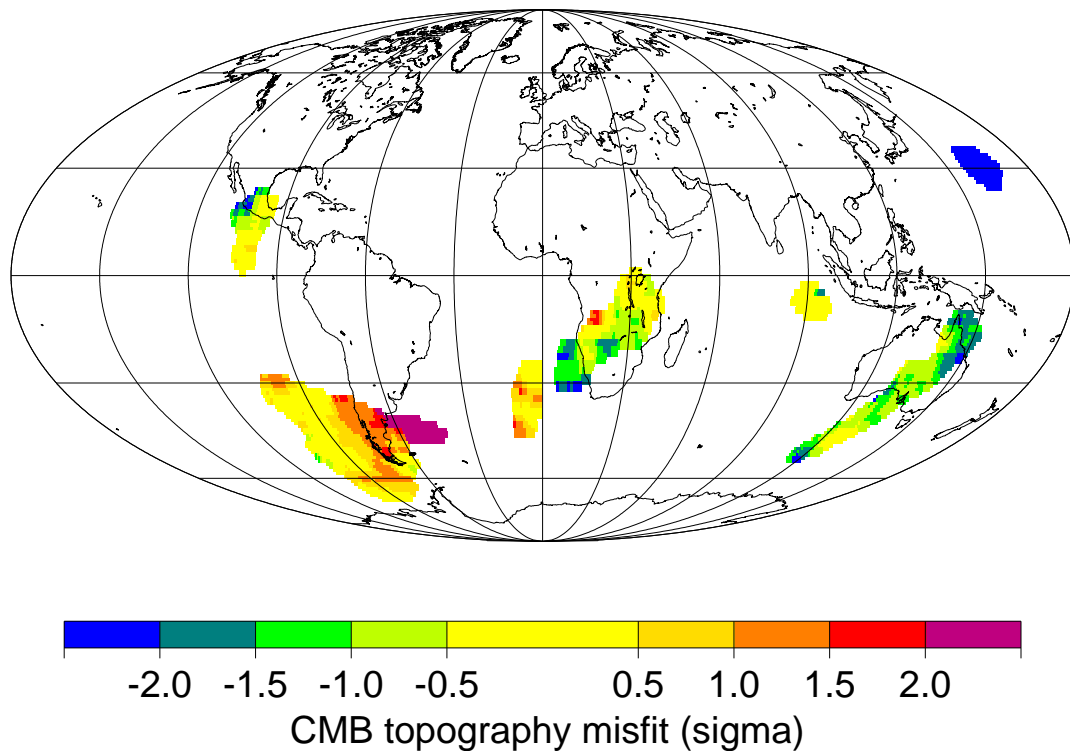
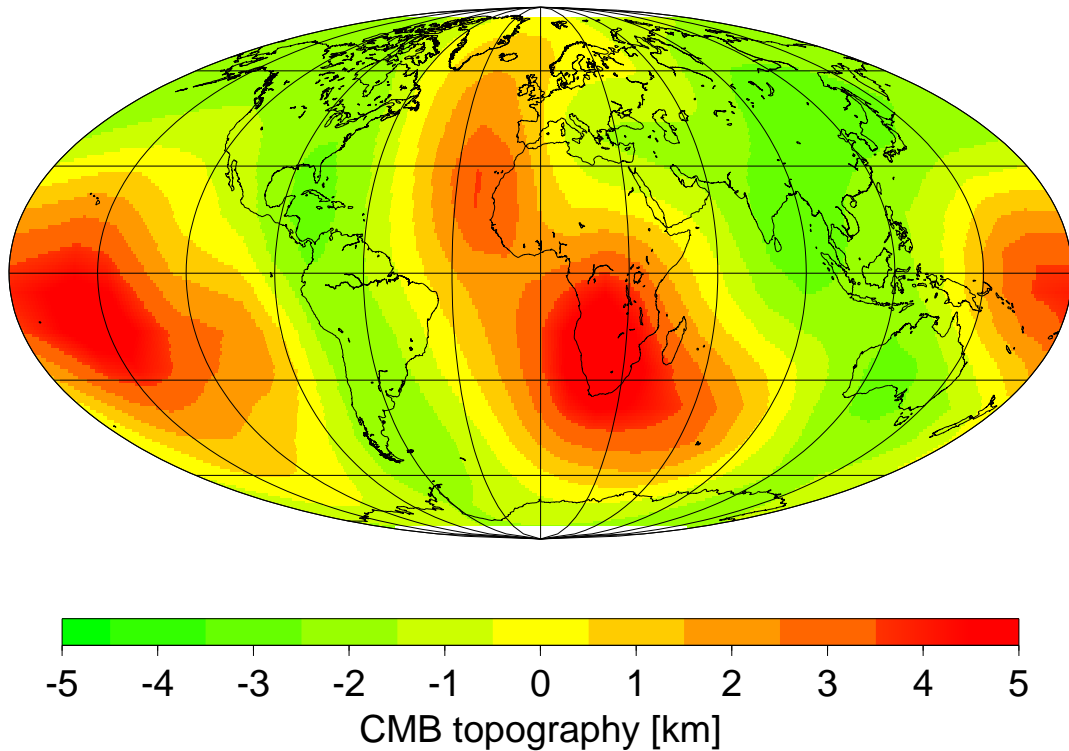
#### B. r.m.s. topography (Garcia and Souriau, 2000)



#### C. excess ellipticity

$490 \pm 110$  m peak-to-valley (from geodetic constraints).

# CMB predictions - no chemical layering



r.m.s. topography 2147 m

excess ellipticity 2237 m peak-to-valley



Interpretation of seismic velocity variations  
in terms of a chemical layer at the base of  
the mantle

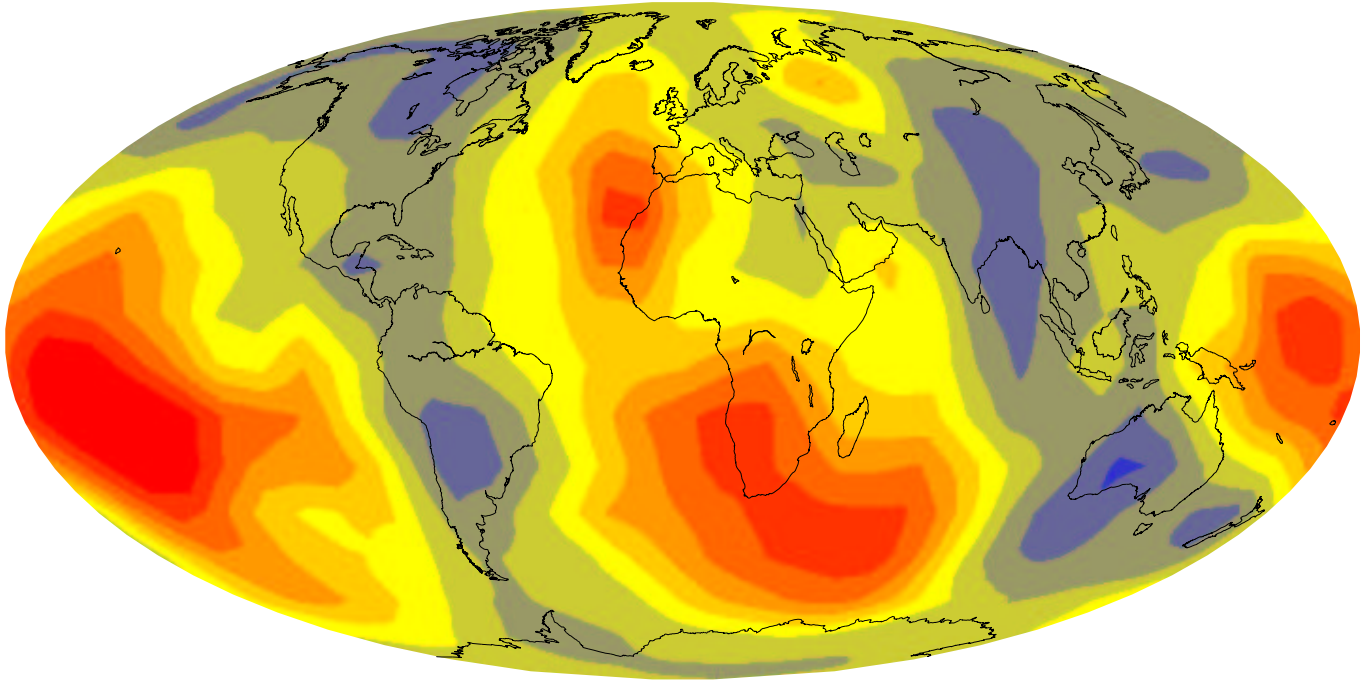
$$\begin{aligned}\frac{\delta v_s}{v_s} &= \frac{1}{\alpha_{s,th}} \frac{\delta \rho}{\rho}_{th} + k_s \delta h \\ \frac{\delta v_c}{v_c} &= \frac{1}{\alpha_{c,th}} \frac{\delta \rho}{\rho}_{th} + k_c \delta h\end{aligned}$$

$\delta v_s$  and  $\delta v_c$  are vertical averages below 2600 km (bottom two layers)

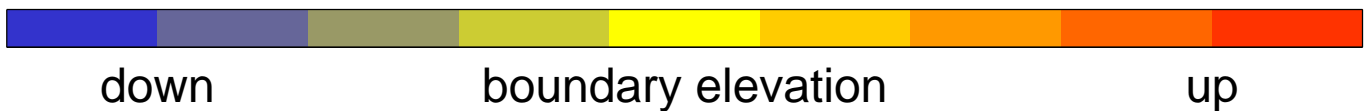
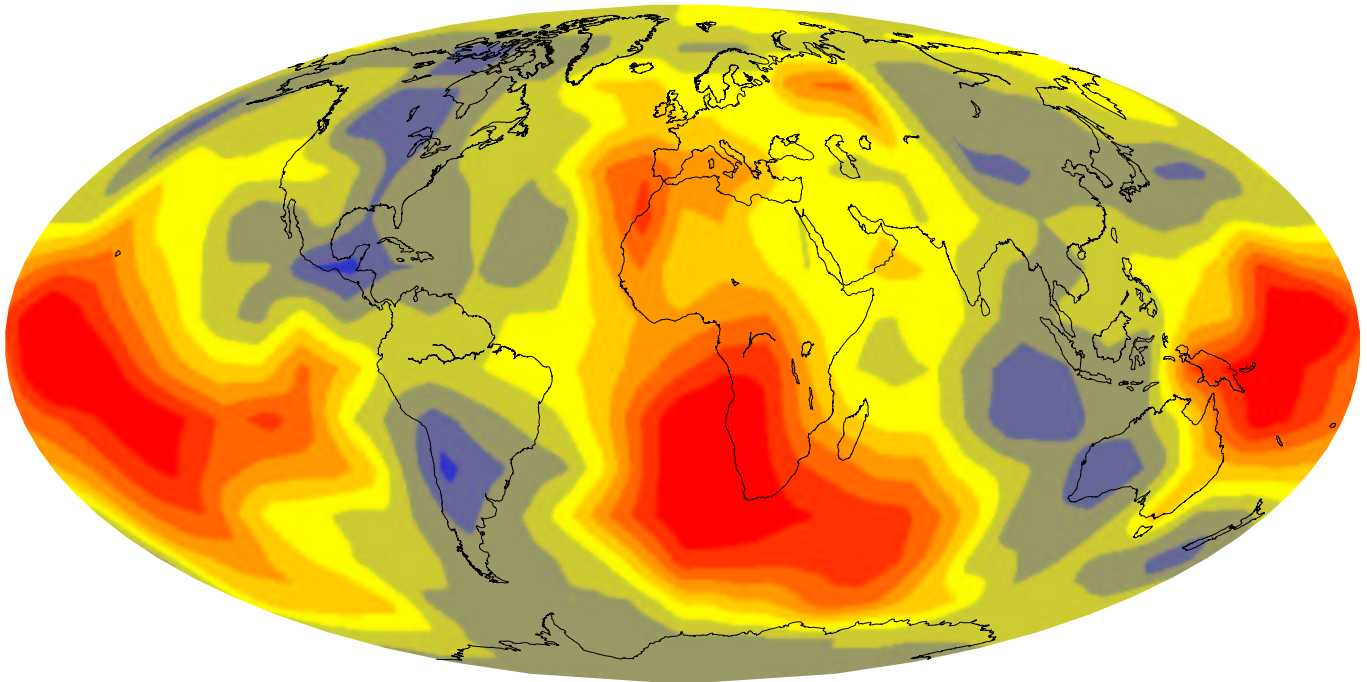
$$\begin{aligned}\delta h &= \left( \frac{\delta v_c}{v_c} - \frac{\alpha_{s,th}}{\alpha_{c,th}} \frac{\delta v_s}{v_s} \right) \left( k_c - k_s \frac{\alpha_{s,th}}{\alpha_{c,th}} \right)^{-1} \\ \frac{\delta \rho}{\rho}_{th} &= \frac{\delta v_s}{v_s} \cdot \alpha_{s,th} - k_1 \cdot \alpha_{s,th} \cdot \left( \frac{\delta v_c}{v_c} - \frac{\alpha_{s,th}}{\alpha_{c,th}} \frac{\delta v_s}{v_s} \right)\end{aligned}$$

$k_1 := k_s \cdot \left( k_c - k_s \frac{\alpha_{s,th}}{\alpha_{c,th}} \right)^{-1}$  is additional free parameter.  
Optimum value  $k_1 = 0.56$

Deflection of lowermost mantle chemical boundary  
inferred from  $v_s$  and  $v_c$  (Masters et al., 2000)  
From flow model

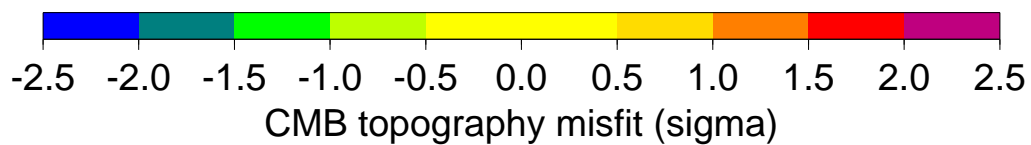
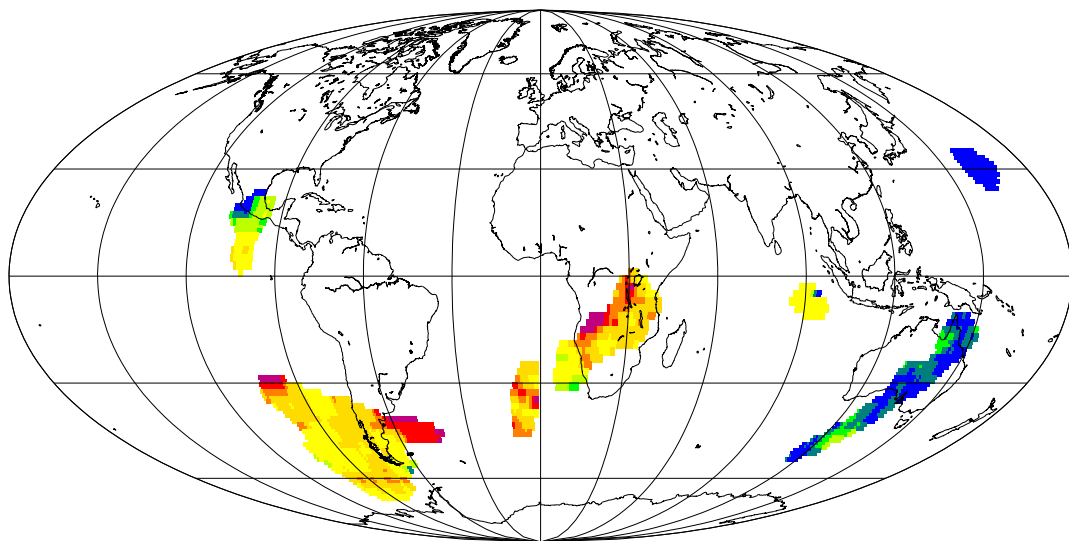
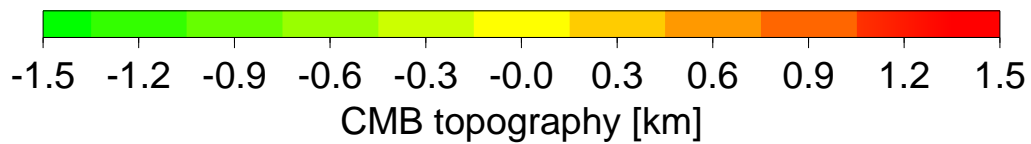
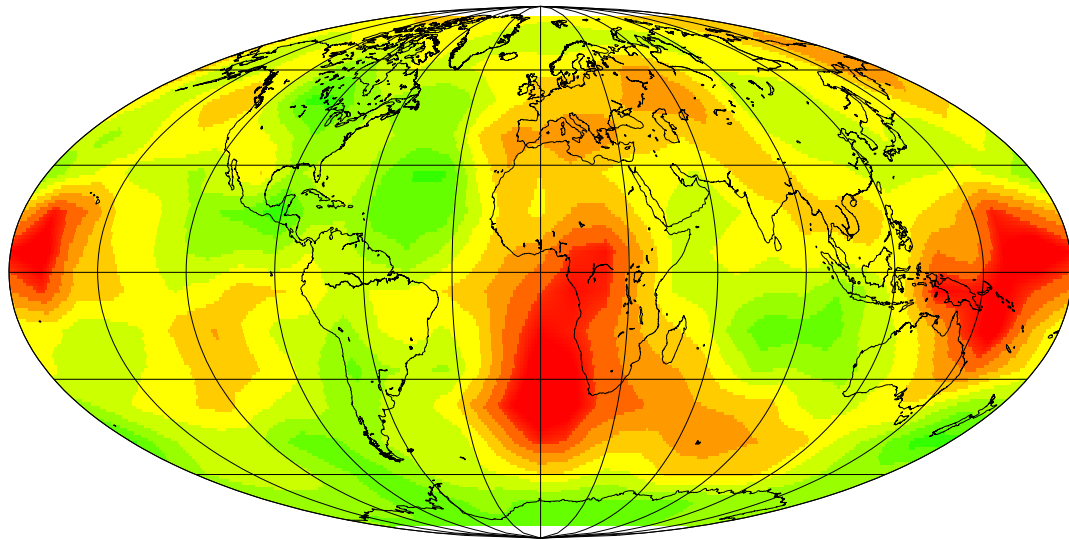


Directly from tomography model



Correlation coefficient = 0.90

# CMB predictions - chemical layering at $0.59 r_E$

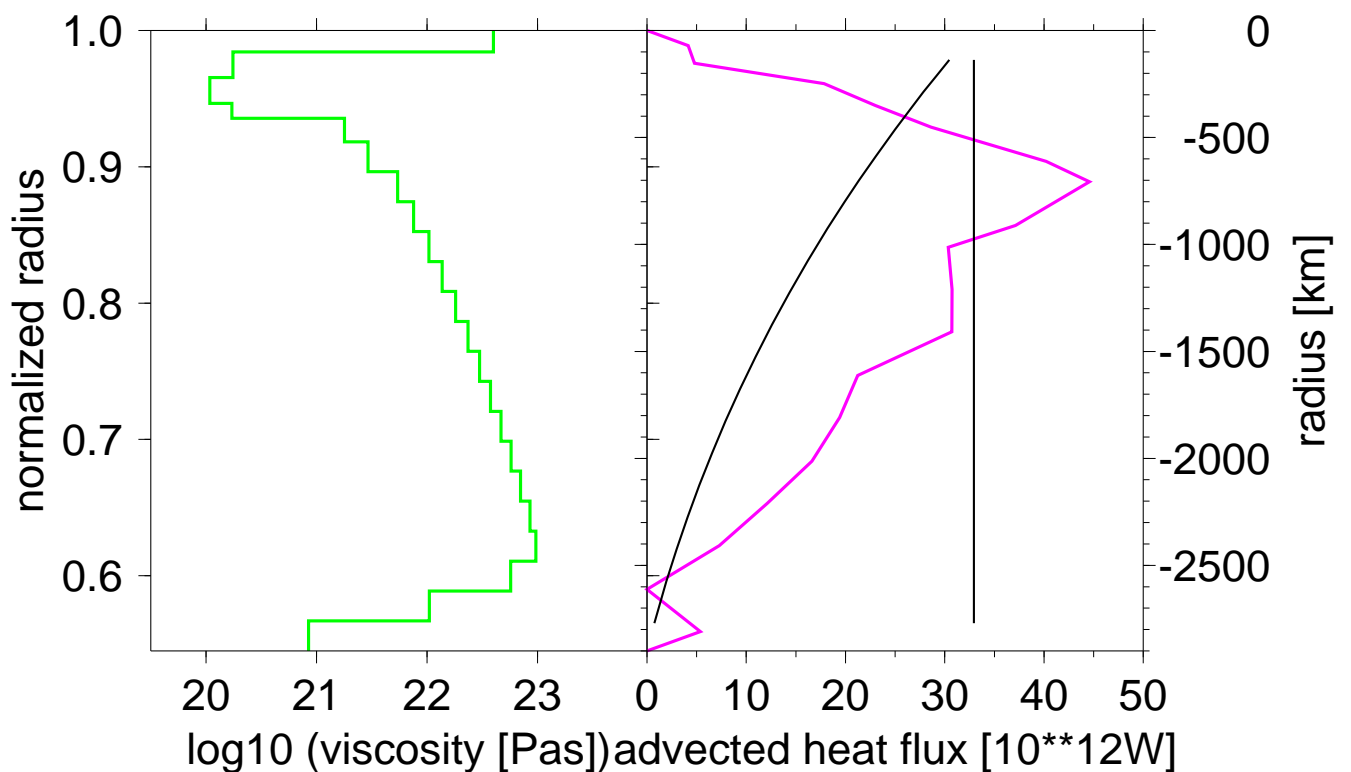
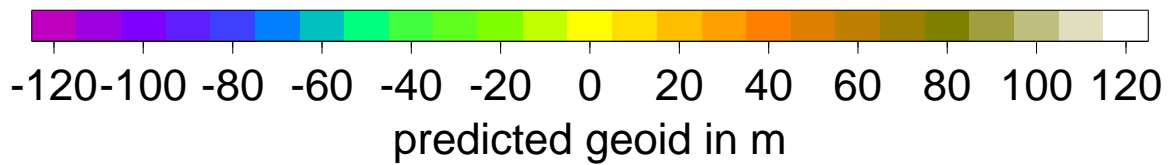
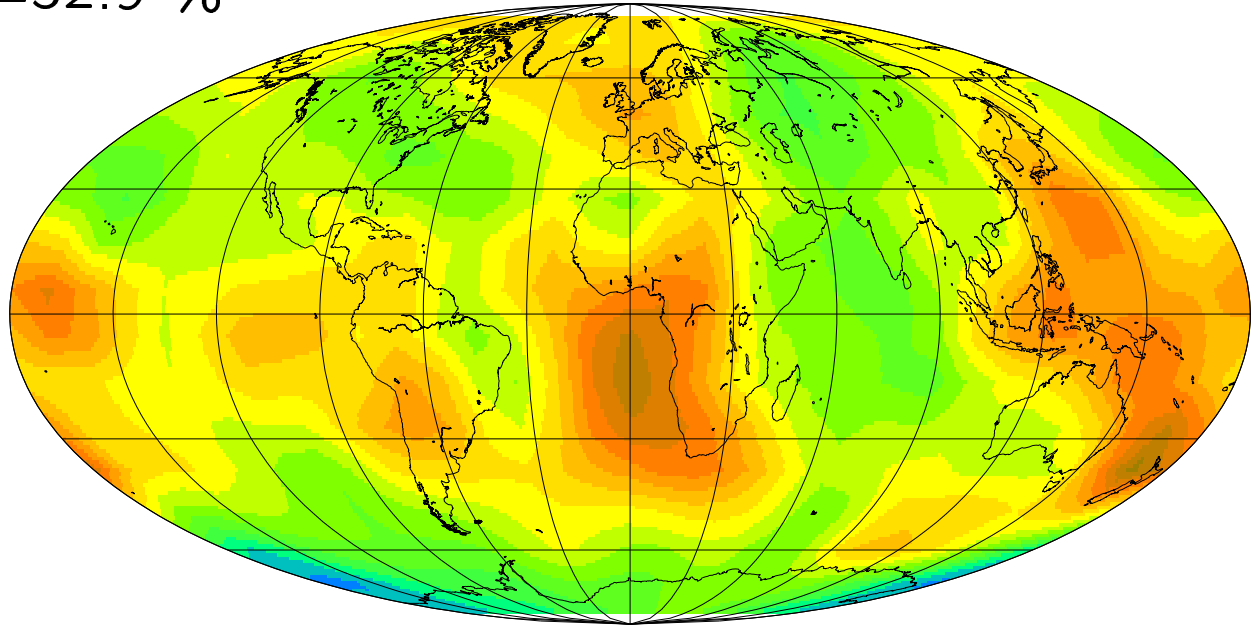


r.m.s. topography 576 m

excess ellipticity 507 m peak-to-valley

# Geoid and heat flux predictions - layering at $0.59 r_E$

VR=52.9 %



## Summary

- Mantle flow model derived from s-wave tomography in accordance with geoid, global heat flux, postglacial rebound – strong increase of viscosity with depth required, *but* . . .
- . . . These models tend to over-predict CMB excess ellipticity and long-wavelength r.m.s. CMB topography – *Therefore* . . .
- . . . we consider both s-wave and bulk sound velocity anomalies, and assume that decorrelation between bulk sound and shear wave anomalies in the lowermost mantle is due a chemically distinct layer of variable thickness at the base of the mantle.
- Thickness variations directly inferred from the tomography model are highly correlated with thickness variations computed with the flow model (correlation coefficients about 0.9).
- We are now able to reasonably fit CMB excess ellipticity and long-wavelength r.m.s. CMB topography as well, *but* . . .
- CMB topography point constraints are still not well fit. Also, in contrast to observations, modeled r.m.s. CMB topography does not significantly increase if shorter wavelengths are considered.
- Both may indicate that the input density model is less accurate at shorter wavelength